DOI: 10.1002/((please add manuscript number))
Article type: Communication

Title: Amplitude Modulation of Anomalously-Refracted Terahertz Waves with Gated-Graphene Metasurfaces

Teun-Teun Kim†, Hyunjun Kim†, Mitchell Kenney, Hyun Sung Park, Hyeon-Don Kim, Bumki Min and Shuang Zhang**
†These authors contributed equally to this work.
*Correspondence and requests for materials should be addressed to these authors.

Dr. Teun-Teun Kim, Prof. Shuang Zhang,
Metamaterials Research Centre, School of Physics and Astronomy,
University of Birmingham,
Birmingham, B15 2TT, UK
E-mail: s.zhang@bham.ac.uk

Dr. Teun-Teun Kim
Center for Integrated Nanostructure Physics
Institute for Basic Science (IBS)
Sungkyunkwan University
Suwon 16419, Republic of Korea

Hyunjun Kim, Hyun Sung Park, Hyeon-Don Kim, Prof. Bumki Min,
Department of Mechanical Engineering,
Korea Advanced Institute of Science and Technology (KAIST),
Daejeon 34141, Republic of Korea
E-mail: bmin@kaist.ac.kr

Dr. Mitchell Kenney
Electronic and Nanoscale Engineering, School of Engineering
University of Glasgow
Glasgow, G12 8LT, UK

Keywords: Metasurfaces, Graphene, Terahertz, Reconfigurable Circular polarization Conversion, Reconfigurable Anomalous Refraction

Metamaterials, which consist of arrangement of deep-subwavelength optical components, have attracted growing attention due to their highly unusual properties and functionalities such as zero and negative index of refraction [1-7], invisibility cloaking [8-10], super-imaging [11-13], and giant chirality [14-16]. Despite the fact that metamaterials in their three-dimensional (3D) forms have been successful in introducing an array of novel potential applications and fundamental physics, it is still a big challenge to achieve practical metamaterials for real-world applications – primarily due to their bulky size, unavoidable material losses, and fabrication

difficulties. Metasurfaces, two dimensional counterparts of metamaterials that consist of 2D array of planar metallic or dielectric structures, have shown great promise for practical applications owing to their exceptional capability of controlling the wavefront of light [17-20]. With suitable design of the building blocks, metasurfaces are capable of generating phase discontinuities with in-plane gradient, leading to anomalously refracted beam in transmission and/or reflection. Recent progress in metasurfaces has led to various ultrathin optical devices including flat lenses [21-24], vortex beam generators [23-25], broadband quarter wave plates [26-27], efficient surface plasmon couplers [28], 3D and high-efficiency holograms [29-32]. The concept of metasurfaces has also been extended to nonlinear optics for manipulating the nonlinearity phase in harmonic generations [33,34].

Although metasurfaces have offered new degrees of freedom for controlling the propagation of light, the amplitude of anomalous refracted waves in metasurfaces is typically fixed by their structural geometry and dimensions, which limits their potential for various applications that require dynamical control over the electromagnetic waves, such as active focusing for lensing and dynamic holography. Active tuning of metasurface requires incorporation of active media whose electromagnetic properties can be changed in real time under external stimuli. Recently, it was shown that anomalous deflection can be dynamically controlled by means of various tuning schemes based on microelectromechanical system (MEMS) [35] and Schottky diode [36]. One suitable candidate for such purpose is graphene, a two-dimensional (2D) form of carbon with the atoms arranged in a honeycomb lattice. Graphene has been studied extensively during the last decade due to its high carrier mobility and unique doping capability originated from its gapless and cone-shaped band structure at the Dirac point. Graphene also shows a gate-controllable light-matter interaction by the shift of the Fermi level, which can be further enhanced by the electromagnetic resonance provided by suitably designed structures [37,38]. Particularly in the Terahertz (THz) regime, strong modulation has been achieved by electrically tuning the density of states available for intraband

transitions [39]. Although significant effort has been devoted to various graphene-based metamaterials for active control of the amplitude and polarization of THz waves in direct transmission [40-43], no research has been carried out on active tuning of beam-steering and focusing with graphene metasurfaces, except in theory [44].

In this paper, we demonstrate gate-controlled THz metasurfaces for amplitude modulation of anomalously refracted waves. The active metasurface is formed by integrating a single layer of graphene onto patterned metasurfaces formed of U-shaped apertures. The Fermi level of the attached chemical vapour deposition (CVD) grown graphene is controlled with a gate voltage, leading to an electrical tuning of the optical conductivity of graphene. By careful design of a spatially linear phase profile, we experimentally demonstrate that the amplitude of anomalously refracted terahertz can be effectively modulated when a voltage is applied to the gate. On the basis of these results, we propose a graphene metalens with a parabolic phase profile and we numerically show that the amplitude of the focused beam can be electrically tuned to a significant extent.

2. Characteristic of metasurface structure

In order to provide a full control over the wave front with the phase variation in the whole range from 0 to 2π, we use a well-studied geometric metasurfaces consisting of U-type aperture antennas, as in the study by Kang *et al*. [45], as illustrated in **Figure 1**a. When considering a coordinate-basis that is locally fixed to the unit cell, the x- and y-polarizations are decoupled. Therefore, only T_{xx} and T_{yy} is used without cross-polarized components (T_{xy}, T_{yx}) to represent the complex transmission coefficient for the two linear polarizations respectively (details are given in the supporting information **Fig. S**1). Here T_{ij} represent the transmission amplitude coefficients, where the first subscript indicates the polarization state of the transmitted wave and the second subscript indicates the polarization of the incident wave. For

the unit-cell rotated by angle θ, the transmission coefficients can be expressed using Jones matrix in the basis of right- and left- handed circular polarization (RCP/LCP) [46]:

$$T_{Cir.} = \begin{bmatrix} T_{RR} & T_{RL} \\ T_{LR} & T_{LL} \end{bmatrix} = \frac{1}{2}\begin{bmatrix} (T_{xx} + T_{yy}) & (T_{xx} - T_{yy})e^{i2\theta} \\ (T_{xx} - T_{yy})e^{-i2\theta} & (T_{xx} + T_{yy}) \end{bmatrix}. \quad (1)$$

For an incident plane wave of left-handed circular polarization, the transmitted field $\boldsymbol{E}_t$ can be obtained from Equation (1) by,

$$\mathbf{E}_t = \frac{1}{2}(T_{xx} + T_{yy}) + \frac{1}{2}(T_{xx} - T_{yy})e^{i2\theta}. \quad (2)$$

It is shown that the cross-polarized component possesses a phase discontinuity $e^{i2\theta}$, which is a Pancharatnum-Berry (PB) phase that has been extensively studied [47,48]. Thus, the wavefront of the cross polarized wave across the metasurface can be precisely controlled by the orientation angle (θ) of each U-shaped aperture. As shown schematically in **Figure 1**b**,** the graphene metasurface device consists of five layers: 1) a polyimide layer as substrate, 2) a metallic metasurface layer, 3) a graphene layer, 4) a square ring electrode and 5) an ion-gel layer as a gate-dielectric material. The fabrication of the graphene metasurface device is carried out by typical micro-fabrication techniques and a chemical vapor deposition (CVD) grown graphene transfer method (see Experimental Section). During the synthesis and fabrication processes, CVD-grown graphene easily becomes p-doped [49], which is also the case for our graphene samples. To apply gate voltage, a voltage supply is connected to the electrode (**B**) and the graphene layer (**G**) (**Figure 1**c). Our fabricated graphene metasurface devices are characterized by using a fiber-based angular resolved terahertz time-domain spectroscopy (THz-TDS) system. A pair of commercially available fiber-based THz photoconductive antennas (Tera15, Menlo System) serve as the THz transmitter and receiver. The transmission coefficients for the circularly cross-polarized lights were obtained through linear polarization measurements with wire grid polarizers (see Experimental Section).

We first investigate electrical modulation of circular polarization conversion in a graphene metasurface with homogeneous unit cells (**Figure 2**a). **Figure 2**b shows the measured

transmission spectra for the circularly cross-polarized wave T_{RL} as a function of the gate voltage V_g (from 0.0 V to 3.0 V). It is shown that by decreasing the gate voltage from the charge neutral point (CNP) (V_{CNP} = 2.2 V, dashed line) where the graphene is most resistive, to the highest doping level (V_{MAX} = 0.0 V) in graphene, the transmission of T_{RL} is reduced because a gate-induced increase in the carrier density of graphene results in a stronger absorption of THz waves through the intraband transitions [39]. To quantify the active tuning capability, measured relative modulation depth for T_{RL} defined by ΔT_{RL} / $T_{RL,\,CNP}$ (where $\Delta T_{RL} = T_{RL} - T_{RL,\,CNP}$) are plotted as a function of V_g (**Figure 2**c). The maximum modulation depth for T_{RL} is measured to be 35 % at f = 1.15 THz. To interpret our experimental results and analyze the electrical tuning mechanism, we perform numerical simulations using the commercial finite element method (FEM) solver CST Microwave Studio. In the numerical simulation, the optical conductivity of graphene was calculated by the Kubo formula as a function of the Fermi level [39]. The applied gate voltage is related to the Fermi level of graphene as $|E_F| = \hbar v_F(\pi N)^{1/2}$. Here v_F is the Fermi velocity, N is the total carrier density given by $N = (n_0^2 + \alpha^2|\Delta V_g|^2)^{1/2}$, and $\alpha \approx 3.5 \times 10^{12}$ cm^{-2}V^{-1} is the gate capacitance in the electron charge. It is assumed that the intraband scattering time τ = 31 fs and the carrier density at the conductivity minimum n_0 = 5.5 × 10^9 cm^2. It is worth to mention that the large specific capacitance of the ion-gel layer is obtained as a result of the thin electric double layer (EDL) which functions as a capacitor [50]. Inserting these values into the Kubo formula, T_{RL} (**Figure 2**d) and ΔT_{RL} / $T_{RL,\,CNP}$ (**Figure 2**e) are calculated as a function of gate-voltage. For a better understanding of the gate-dependent modulation characteristics, measured modulation depth ΔT_{RL} / $T_{RL,\,CNP}$ at the frequency 1.15 THz are plotted in **Figure 2**f as a function of $|\Delta V_g|^{1/2}$ and compared with the simulation results. It is shown that the modulation depth is proportional to the square root of the gate voltage, as shown in our previous work [40].

We next demonstrate gate-dependent modulation on anomalously refracted THz wave from a graphene metasurface with a linear phase profile. The anomalous refraction angle for circularly cross-polarized light can be predicted by the generalized Snell's laws [17-19]

$$n_t \sin \alpha_t - n_i \sin \alpha_i = \frac{\lambda}{2\pi} \frac{\mathrm{d}\Phi}{\mathrm{d}x} \quad (3)$$

Where α_i and α_t are the incident and refracted angle of the plane wave, n_i and n_t are the refractive index in the incident and transmitted media, respectively. For a THz wave at normal incidence onto the metasurface and refracted into air (i.e. $n_t = 1$), the anomalous refraction angle can be calculated as $\sin \alpha_t = (\lambda/2\pi)\, \mathrm{d}\Phi/\mathrm{d}x$. **Figure 3**a shows a supercell of the refracting metasurface, which consists of 11 antennas with a discrete rotation step of 18° to cover a PB phase variation of 2π (**Figure 3**b). The full-wave simulation at 1.15 THz at two different gate voltages of V_g = 2.2 V and V_g = 0.0 V was performed for an RCP transmitted THz wave, converted from an incident LCP wave propagating along the z-axis at normal incidence (**Figure 3**c). A tilted wavefront resulting from the in-plane phase gradient is clearly observed in the simulation and it is further shown that the amplitude of the refracted transmission is strongly modified by the variation of the applied voltage. It is worth to mention that although the transmission phase is also modulated by changing the conductivity of graphene layer, the modulated phase remains linear phase profile, and therefore, only the amplitude of anomalously refracted waves can be modulated without distorting the wave shape and direction (see supporting information, **Fig. S**2).

To experimentally demonstrate electrical amplitude modulation of the anomalously refracted waves, we fabricated a graphene metasurface with a linear phase gradient. An optical microscope image of the fabricated sample is shown in **Figure 4**a. The relationship between the measured refraction angle α_t for the circularly cross-polarized wave and its frequency is shown in **Figure 4**b. The results show good agreement with the theoretical results predicted by Equation (3). At 1.15 THz, the circularly cross-polarized transmission (**Figure 4**c) shows a

maximum of 30 % at $\alpha_t = 20°$. The measured transmission spectra for T_{RL} through the graphene metasurface as a function of gate voltage V_g (from 3.0 V to 0.0 V) is shown in **Figure 4**d. It is observed that the refracted circularly cross-polarized THz wave is effectively controlled by the variation of an applied voltage. The maximum modulation depth for refracted T_{RL} is measured to be 28 % at the frequency 1.15 THz (**Figure 4**e).

Besides the anomalous refraction, the amplitude of focused cross-polarized light can also be electrically controlled by gating. For a certain focal length *f*, a focusing lens can be designed with spatially parabolic phase profile

$$\emptyset(x) = 2\pi f/\lambda - (2\pi\sqrt{(f^2 + x^2)})/\lambda. \quad (4)$$

With such a parabolic profile, the incident wave can be focused with a focal length *f*. To realize the parabolic phase variation in Equation (4), a metasurface array composed of 19 rotating resonators with defined rotation angle is shown in **Figure 5**a. In our study, we set $f = 11a$, and $x = na$ with the periodicity $a = 76\ \mu$m and $n = 0, \pm1 \sim \pm9$. To confirm the dynamically tunable metalens, we numerically calculated the electric field and energy density distribution at the operation frequency 1.15 THz with different gate voltages. As shown in **Figure 5**b, in the case of V_{CNP} for LCP incidence, the wave front of transmitted RCP wave can be converged well. The focal point is at 845 μm which agrees well with the original design at 836 μm. It can be seen that by increasing voltage to 2.2 V, the field amplitude and energy density at the focal point is significantly reduced.

5. Conclusion

In conclusion, we fabricated electrically tunable graphene metasurfaces with linear phase variation and demonstrated that the anomalously refracted circularly cross-polarized THz waves can be modified by an applied gate voltage. The measurement on the fabricated device shows that a modulation depth up to 28 % for refracted THz waves can be observed at a

relatively small gate voltage of below 3 V. Furthermore, we numerically demonstrated that the focused THz wave from metasurfaces with a parabolic phase variation can be electrically controlled by changing the optical conductivity of graphene. Benefitting from the electrically tunable amplitude modulation of anomalous refraction and focusing in deep-subwavelength scale (~λ/10), the graphene metasurfaces can be used as active flat half wave plates and lenses, which may have potential applications in THz telecommunications, high resolution terahertz displays, and advanced THz imaging devices.

Experimental Section

Sample fabrication: The fabrication procedure of graphene metasurface devices was achieved by typical micro-fabrication techniques and a chemical vapor deposition (CVD) grown graphene transfer method. First, to form a flexible substrate, polyimide solution (PI-2610, HD MicroSystems) was spin coated with the target thickness of 1 μm on a sacrificial silicon wafer, and the polyimide solution was fully cured subsequent two-step baking process in a convection oven and a furnace. All metallic structures (meta-atom layer, electrode component) were composed of 100-nm-thick gold (Au) with a 10-nm-thick chromium (Cr) adhesion layer from conventional electron-beam (E-beam) evaporation. Monolayer graphene (Graphene Square, Inc.) on copper foil grown by a chemical vapor deposition (CVD) process is directly transferred onto the metasurface layer by typical thermal release tape (TRT) method. As a gate dielectric, we employed 20-μm-thick ion-gel using cut and stick method [51]. The ion-gel solution was prepared by dissolving P(VDF-HFP) and [EMI][TFSA] in acetone with weight ratio of 1:4:7. This solution was dried in a vacuum oven at a temperature of 70°C during 24 hours. The cured ion-gel was cut with a razor blade, and then transferred between two electrodes. At last, the phase-variant graphene metasurface device were acquired by peeling off the device from the silicon substrate. The device is attached onto a printed circuit board (PCB) component.

THz TDS measurement: Since the signals from the THz antenna were linearly polarized, the transmission amplitude for the linearly polarized waves were measured as T_{xx}, T_{xy}, T_{yx}, and T_{yy} by using four wire grid polarizers. Here, the first subscript indicates the polarization (x or y) of the transmitted wave and the second subscript indicates the polarization of the incident wave. From the transmission amplitude calculated in a linear basis, the circularly cross-polarized transmission amplitude T_{RL} can be obtained as $T_{RL} = \{(T_{xx} - T_{yy}) - i(T_{xy} + T_{yx})\} / 2$.

Acknowledgements

T.-T.K and H.K. contributed equally to this work. This work was supported by IBS-R011-D1, National Research Foundation of Korea (NRF) through the government of Korea (MSIP) (Grants No. NRF-2017R1A2B3012364, 2014M3C1A3052537 and, No.2015001948). The work was also supported by the center for Advanced Meta-Materials (CAMM) funded by Korea Government (MSIP) as Global Frontier Project (CAMM 2014M3A6B3063709), the ERC Consolidator Grant (TOPOLOGICAL), and the Royal Society.

Received: ((will be filled in by the editorial staff))
Revised: ((will be filled in by the editorial staff))
Published online: ((will be filled in by the editorial staff))

References

[1] J. B. Pendry, *Phys. Rev. Lett.* **2000**, *85*, 3966.

[2] D. R. Smith, J. B. Pendry, M. C. K. Wiltshire, *Science* **2004**, *305*, 5685.

[3] S. Zhang, W. Fan, N. C. Panoiu, K. J. Malloy, R. M. Osgood, R. J. Brueck, *Phys. Rev. Lett.* **2005**, *95*, 137404.

[4] V. M. Shalaev, W. Cai, U. K. Chettiar, H. K. Yuan, A. K. Sarychev, V. P. Drachev, A. V. Kildishev, *Opt. Lett.* **2005**, *30*, 3356.

[5] X. Huang, Y. Lai, Z. H. Hang, H. Zheng, C. T. Chan, *Nat. Mater.* **2011**, *10*, 582.

[6] Y. Yang, S. Kita, P. Munoz, O. Reshef, D. I. Vulis, M. Yin, M. Loncar, E. Mazur, *Nat. Photonics* **2015**, *9***,** 738

[7] D. Schuig, J. J. Mock, B. J. Justice, S. A. Cummer, J. B. Pendry, A. F. Starr, D. R. Smith, *Science* **2006**, *314*, 977.

[8] J. Valentine, J. Li, T. Zentgraf, G. Bartal, X. Zhang, *Nat. Mater*. **2009**, *8*, 568.

[9] T. Ergin, N. Stenger, P. Brenner, J. B. Pendry, M. Wegener, *Science* **2010**, *328*, 337.

[10] X. Ni, Z. J. Wong, M. Mrejen, Y. Wang, X. Zhang, *Science* **2015**, *349*, 1310.

[11] N. Fang, H. Lee, C. Sun, X. Zhang, *Science* **2005**, *308*, 534.

[12] T. Taubner, D. Korobkin, Y. Urzhumov, G. Shvets, R. Hillenbrand, *Science* **2006**, *313*, 1595.

[13] Z. Liu, H. Lee, Y. Xiong, C. Sun, X. Zhang, *Science* **2007**, *315*, 1686.

[14] J. B. Pendry, *Science* **2004**, *306*, 1353.

[15] S. Zhang, Y. –S. Park, J. Li, X. Lu, W Zhang, X. Zhang, *Phys. Rev. Lett.* **2009**, *102*, 023901.

[16] T. –T. Kim, S. S. Oh, H. –S. Park, R. Zhao, S. –H. Kim, W. Choi, B. Min, O. Hess, *Sci. Rep*. **2014** *4*, 5864.

[17] N. Yu, P. Genevet, M. A. Kats, F. Aieta, J. P. Tetienne, F. Capasso, Z. Gaburro, *Science* **2011**, *334*, 333.

[18] N. Yu, F. Capasso, *Nat. Mater*. **2014**, *13*, 139.

[19] F. Aieta, P.Genevet, M. A. Kats, N. Yu, R. Blanchard, Z. Gaburro, F. Capasso, *Nano Lett.* **2012** *12*, 4932–4936.

[20] X. Chen, L. Huang, H. Mühlenbernd, G. Li, B. Bai, Q. Tan, G. Jin, C. Qiu, S. Zhang, T. Zentgraf, *Nat. Commun.* **2012**, *3*, 1198.

[21] X. Ni, S. Ishii, A. V. Kildishev, V. M. Shalaev, *Lights: Sci. Appl.* **2013**, *2*, 72.

[22] F. Aieta, M. A. Kats, P. Genevet, F Capasso, *Science* **2015**, *347*, 1342

[23] X. Ni, N. K. Emani, A. V. Kildishev, A. Boltasseva, V. M. Shalaev, *Science* **2012**, *335*, 427.

[24] L. Huang, X. Chen, H. Mühlenbernd, G. Li, B. Bai, Q. Tan, G. Jin, T. Zentgraf, S. Zhang, *Nano Lett.* **2012**, *12*, 5750.

[25] X. Zhang, Z. Tian, W. Yue, J. Gu, S. Zhang, J. Han, W. Zhang, *Adv. Mater*. **2013**, *25*, 4567.

[26] S. Sun, Q. He, S. Xiao, Q. Xu, X. Li, L. Zhou, *Nat. Mater.* **2012**, *11*, 426–431.

[27] N. Yu, F. Aieta, P. Genevet, M. A. Kats, Z. Gaburro, F. Capasso, *Nano Lett*. **2012**, 6328-6333.

[28] L. Huang, X. Chen, H. Mühlenbernd, H. Zhang, S. Chen, B. Bai, Q. Tan, G. Ji, K. –W. Cheah, C. –W. Qiu, J. Li, T. Zentgraf, S. Zhang, *Nat. Commun.* **2013**, *4*, 2808.

[29] S. Larouche, Y. –J. Tsai, T. Tyler, N. M. Jokerst, D. R. Smith, *Nat. Mater.* **2012**, *11*, 450-454.

[30] X. Chen, L. Huang, H. Mühlenbernd, G. Li, B. Bai, Q. Tan, G. Jin, C. –W. Qiu, S. Zhang, T. Zentgraf, *Nat. commun.* **2012**, *3*, 1198.

[31] X. Ni, A. V. Kildishev, V. M. Shalaev, *Nat. commun.* **2013**, 4, 2087.

[32] G. Zheng, H. Mühlenbernd, M. Kenney, G. Li, T. Zentgraf, S. Zhang, *Nat. Nanotechnol.* **2015**, *10*, 308-312.

[33] G. Li, S. Chen, N. Pholchai, B. Reineke, P. W. H. Wong, E. Y. B. Pun, K. W. Cheah, T. Zentgraf & S. Zhang, *Nat. Mater.* **2015**, *14*, 607-612.

[34] M. Tymchenko, J. S. Gomez-Diaz, J. Lee, N. Nookala, M. A. Belkin, and A. Alù, *Phys. Rev. Lett.* **2015**, *115*, 207403.

[35] X. Su, C. Ouyang, N. Xu, W. Cao, X. Wei, G. Song, J. Gu, Z. Tain, J. F. O'Hara, J. Han, W. Zhang, *Opt. Exp.* **2015**, *23*, 27152.

[36] L. Cong, P. Pitchappa, Y. Wu, L. Ke, C. Lee, N. Singh, H. Yang, R. Singh, *Adv. Opt. Mater.* **2017**, 5, 1600716.

[37] A. Das, S. Pisana, B. Chakraborty, S. Piscanec, S. K. Saha, U. V. Waghmare, K. S. Novoselov, H. R. Krishnamurthy, A. K. Geim, A. C. Ferrari, A. K. Sood, *Nat. Nanotechnol.* **2008**, *3*, 210-215.

[38] D. K. Efetov, P. Kim, *Phys. Rev. Lett.* **2010**, *105*, 256805.

[39] V. P. Gusynin, S. G. Sharapov, and J. Carbotte, *Int. J. Mod. Phys. B*, **2007**, *21*, 4611-4658.

[40] S. H. Lee, M. Choi, T. –T. Kim, S. Lee, M. Liu, X. Yin, H. K. Choi, S. S. Lee, C. –G. Choi, S. –Y. Choi, X. Zhang, B. Min, *Nat. Mater.* **2012**, *11*, 1-6.

[41] F. Valmorra, G. Scalari, C. Maissen, W. Fu, C. Schönenberger, J. W. Choi, H. G. Park, M. Beck, and J. Faist, *Nano Lett.* **2013**, *13*, 3193–3198.

[42] W. Gao, J. Shu, K. Reichel, D. V. Nickel, X. He, G. Shi, R. Vajtai, P. M. Ajayan, J Kono, D. M. Mittleman, Q. Xu, *Nano Lett.* **2014**, *14*, 1242–1248.

[43] Z. Miao, Q. Wu, X. Li, Q. He, K. Ding, Z. An, Y. Zhang, L. Zhou, *Phys. Rev. X* **2016**, *5*, 041027.

[44] Z. Li, K. Yao, F. Xia, S. Shen, J. Tian, Y. Liu, *Sci. Rep*. **2015**, *5*, 12423.

[45] M. Kang, T. Feng, H. –T. Wang, J. Li, *Opt. Exp.* **2012**, *20*, 15882.

[46] V. A. Fedotov, P. L. Mladyonov, S. L. Prosvirnin, A.V. Rogacheva, Y. Chen, N. I. Zheludev, *Phys. Rev. Lett.* **2006**, *97*, 167401.

[47] X. Chen, L. Huang, H. Muhlenbernd, G. Li, B. Bai, Q. Tan, G. Jin, C.-W. Qiu, S. Zhang, T. Zentgraf, *Nat. Commun.* **2012**, *3*, 1198.

[48] M. Kenney, S. Li, X. Zhang, X. Su, T. –T Kim, D. Wang, D. Wu, C. Ouyang, J. Han, Weili Zhang, H. Sun, and S. Zhang, *Adv. Mater*. **2016**, *28*, 9567.

[49] A. Pirkle, J. Chan, A. Venugopal, D. Hinojos, C. W. Magnuson, S. McDonnell, L. Colombo, E. M. Vogel, R. S. Ruoff, R. M. Wallace, *Appl. Phys. Lett.* **2011**, *99*, 122108.

[50] V. Narasimhan, Sung-Yong Park, *Langmuir* **2015**, *31*, 8512−8518.

[51] K. H. Lee. M. S. Kang, S Zhang, Y. Gu, T. P. Lodge, C. D. Frisbie, *Adv. Mater.* **2012**, *24*, 4457–4462.

< Title candidate List of this paper >

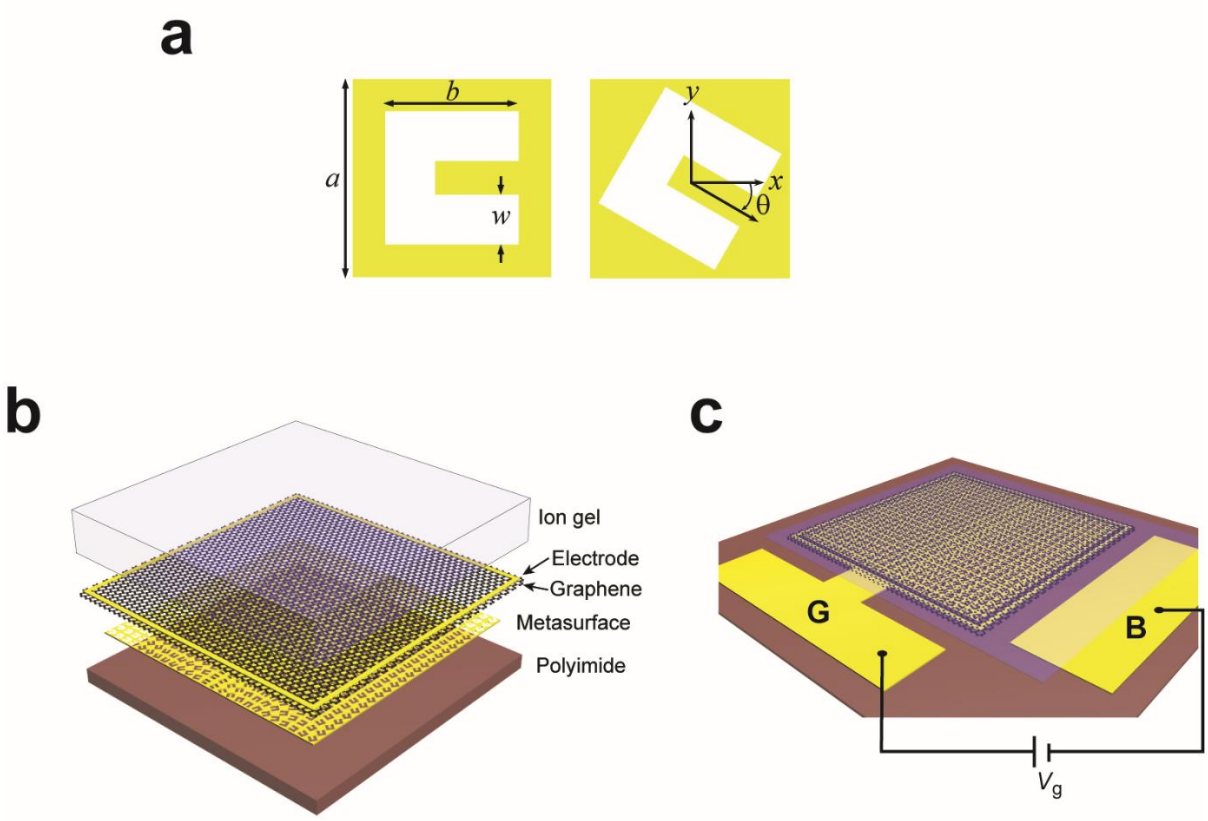

Figure 1. a) Unit-cell structure of U-shape aperture with the dimensions indicated in the figure: a = 76 μm, b = 51 μm, w = 19 μm, and the rotational angle θ. b) Schematic rendering of active graphene metasurfaces composed of a single layer of graphene deposited on the layer of U-shape apertures. For a gate-controllable conductivity of graphene, an ion-gel layer (thickness t_{ion} = 20 μm) and square ring electrode are incorporated to the graphene layer. c) Fabricated graphene metasurfaces. **B** is a base connected to the ion-gel and **G** is a gate connected to the graphene layer.

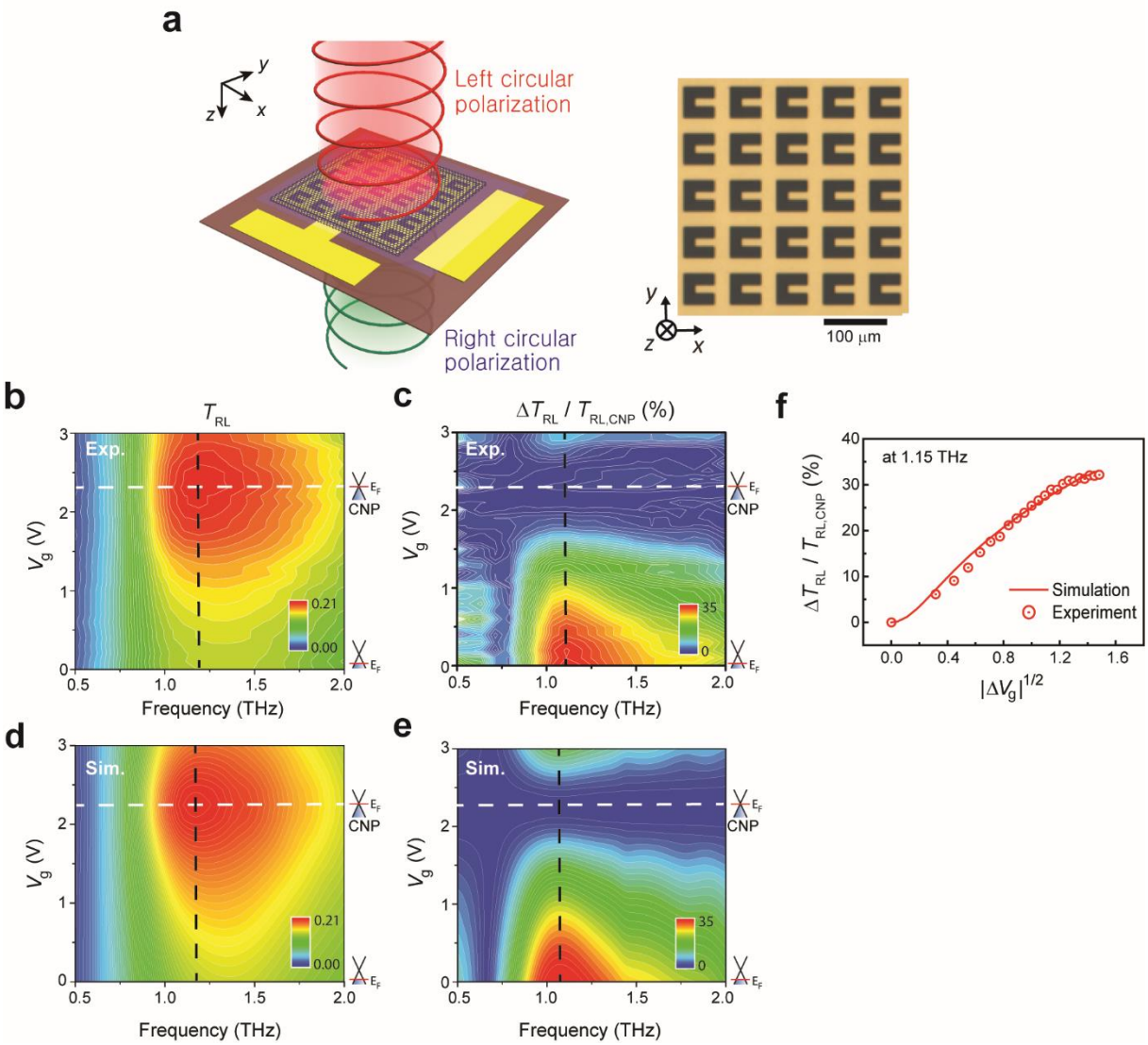

Figure 2. a) Schematic view and optical micrograph image of active circular polarization converter, in which a normally incident left handed circular polarized wave is converted into a right handed circular polarized one. Cross-polarized transmittance T_{RL} obtained by b) experimental measurements and d) numerical simulation, and c) measured and e) simulated relative modulation depth for T_{RL} as a function of V_g. f) Measured modulation depth for T_{RL} (scatter) plotted as a function of $|\Delta V|^{1/2}$ along with the simulated modulation curve (line) at the frequency 1.15 THz.

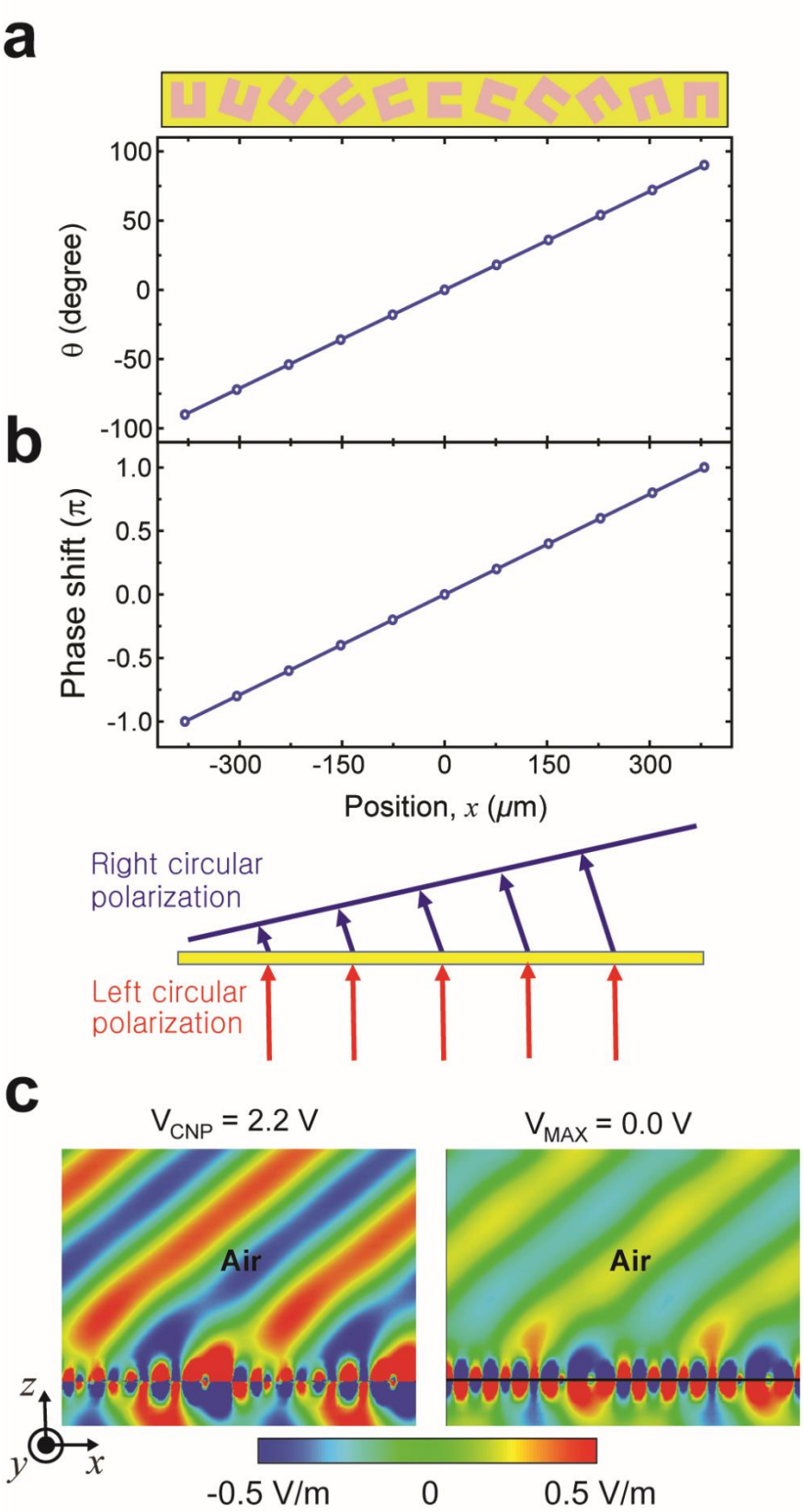

Figure 3. a) Schematic of the metasurface supercell for linear phase variation consists of 11 antennas with discrete rotation step θ = 18°. b) Phase shift for left-handed circularly polarized (LCP) transmission of the proposed structure under right-handed circularly polarized (RCP) incidence at 1.15 THz. A normally incident LCP wave is converted to a RCP transmission wave. c) Simulated *y*-component of electric field distributions for LCP incidence with two different gate voltages.

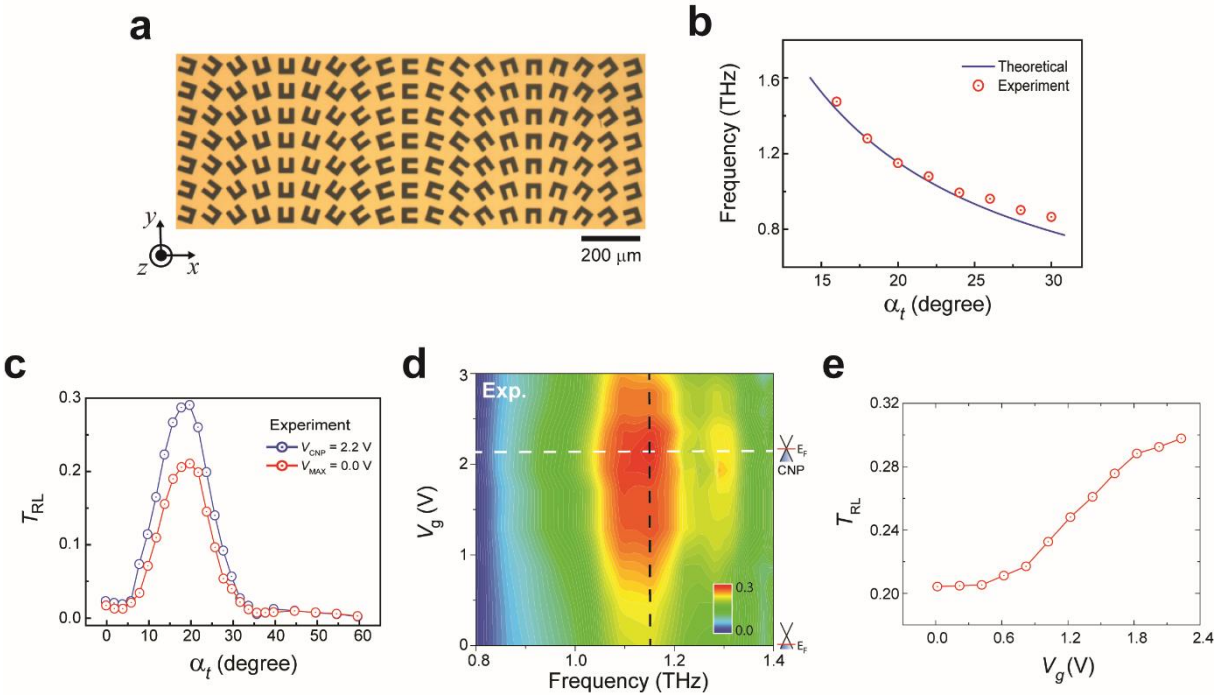

Figure 4. a) Fabricated supercell image of graphene metasurfaces for electrically tunable anomalous refraction. b) Comparison between measured and theoretical results of refraction angle for cross-polarized light α_t with different frequencies at CNP. c) Measured cross-polarized transmission T_{RL} at 1.15 THz under normal incidence as a function of angle α_t with two different gate voltages, d) T_{RL} at $\alpha_t = 20°$ as a function of gate voltage V_g, and e) modulation depth at 1.15 THz for refracted T_{RL} plotted as a function of V_g.

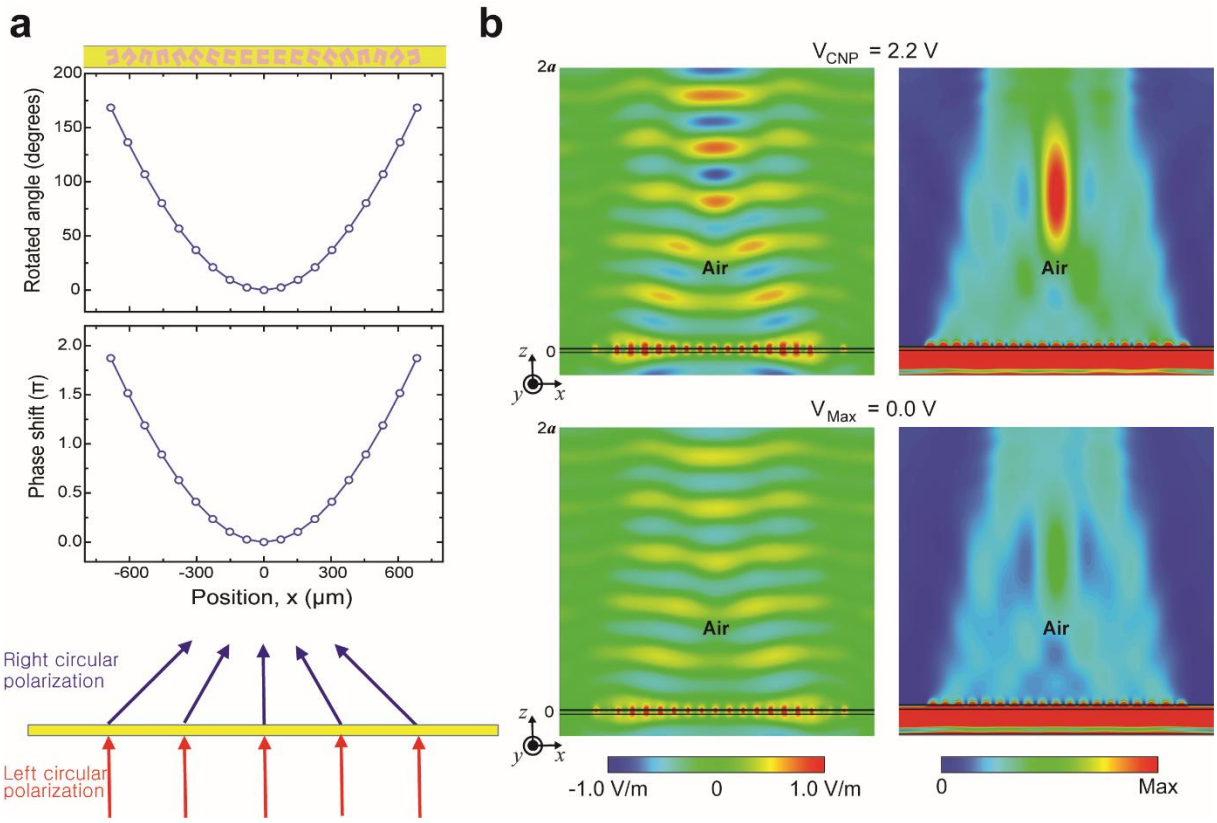

Figure 5. Amplitude modulation of focused THz waves with gated-graphene metasurfaces a) Supercell of graphene metasurfaces composed of resonators with 19 different rotated angle for parabolic phase profile. b) (left) Electric field and (right) energy density distribution at 1.15 THz with different gate voltages.

Keyword Metasurfaces, Graphene, Terahertz, Reconfigurable Circular polarization Conversion, Reconfigurable Anomalous Refraction

Teun-Teun Kim†, Hyunjun Kim†, Mitchell Kenney, Hyun Sung Park, Hyeon-Don Kim, Bumki Min* and Shuang Zhang*

Title Amplitude Modulation of Anomalously-Refracted Terahertz Waves with Gated-Graphene Metasurfaces

ToC figure ((Please choose one size: 55 mm broad × 50 mm high **or** 110 mm broad × 20 mm high. Please do not use any other dimensions))

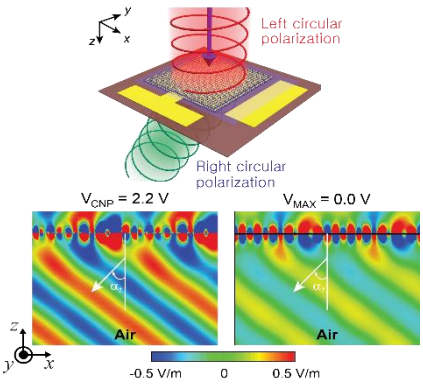

((Supporting Information can be included here using this template))

Supporting Information

Title Electrically-Tunable Anomalously-Refracted Terahertz Waves with Graphene Metasurfaces

Teun-Teun Kim†, Hyunjun Kim†, Mitchell Kenney, Hyun Sung Park, Hyeon-Don Kim, Bumki Min and Shuang Zhang**

When considering a coordinate-basis that is locally fixed to the unit cell as shown in Fig. **S1** a, the x-polarized and y-polarized components are decoupled; thus, there are no linearly cross-polarized components (T_{xy}, T_{yx}). In other words, the transformation matrix is coordinate-basis dependent. If the unit cell is rotated with rotation angle θ as shown in Fig. **S1** b, the cross-polarized components exist. However, since the incident light is circulaly polarized,the original coordinate-basis can be also rotated with θ. In this new coordinate-basis, there are no coross polarized components either. The angle between the two coordinate-bases is related to the geometric (Pancharatnam-Berry phase), which is simply a phase term attached to the transmission matrix ($e^{i2\theta}$ and $e^{-i2\theta}$) for the T_{RL} and T_{LR} terms (as given in the manuscript, equation 1). For a simple calculation to eliminate the cross-polarized components, the local coordinate-basis and an extra phase term is used to equivalently describe the realistic case.

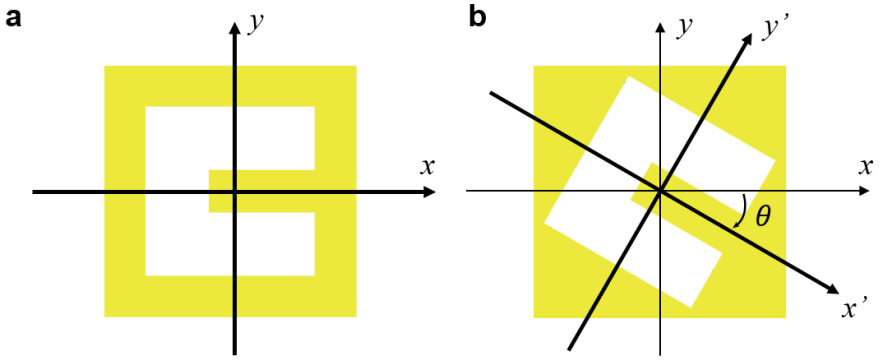

Fig. S1

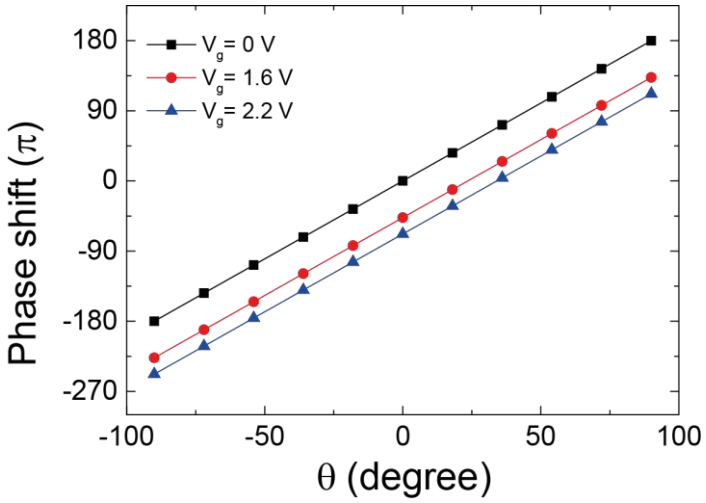

Fig. S2 Phase shift for T_{RL} at 1.15 THz with three different gate voltages.